

# Modeling the emission line sequence of H II galaxies

G. Stasińska<sup>1</sup> and Y. Izotov<sup>2</sup>

<sup>1</sup> LUTH, Observatoire de Meudon, 5 Place Jules Janssen, F-92195 Meudon Cedex, France

<sup>2</sup> Main Astronomical Observatory, Ukrainian National Academy of Sciences, Kyiv 03680, Ukraine  
e-mail: izotov@mao.kiev.ua

Received ???; accepted ???

**Abstract.** Using a sample of unprecedented size (about 400 objects) of H II galaxies in which the oxygen abundances have been obtained using the temperature derived from the [O III]  $\lambda 4363/5007$  line ratio, we confirm that the H II galaxies form a very narrow sequence in many diagrams relating line ratios and H $\beta$  equivalent width. We divide our sample in three metallicity bins, each of which is compared with sequences of photoionization models for evolving starbursts with corresponding metallicity. Our aim is to find under what conditions a theoretical sequence can reproduce all the observed trends. Taking into account the presence of an older, non-ionizing stellar population, for which independent indications exist, we find that the simple model of an adiabatic expanding bubble reproduces the observational diagrams very well if account is taken of an aperture correction and the covering factor is assumed to decrease with time exponentially with an e-folding time of 3 Myr. We find that the He II  $\lambda 4686$  nebular line emission occurs too frequently and in too wide a range of  $EW(H\beta)$  to be attributable to either the hard radiation field from Wolf-Rayet stars or the X-rays produced by the latest stellar generation. Assuming that the He II  $\lambda 4686$  line is due to photoionization by a hot plasma at a temperature of  $10^6$  K, a total X-ray luminosity of  $10^{40} - 4 \times 10^{40}$  erg s<sup>-1</sup> is required for at least half of the sources. We find evidence for self-enrichment in nitrogen on a time scale of several Myr, and argue for a possible self-enrichment in oxygen as well.

**Key words.** galaxies: abundances – galaxies: ISM – galaxies: starburst – ISM: H II regions

## 1. Introduction

It has been known for a long time that giant H II regions form a well defined sequence in emission line diagnostic diagrams (McCall et al. 1985; Veilleux & Osterbrock 1987). The first interpretations of this sequence were based on single star photoionization models, and it was concluded that the driving parameter of the sequence is the metallicity, and that variations of an additional parameter – either the effective temperature of the ionizing stars or the ionization parameter – are required in order to reproduce the observed sequence (McCall et al. 1985; Dopita & Evans 1986).

However, giant H II regions are powered by intensive bursts of star formation (e.g. Sargent & Searle 1970; Mas-Hesse & Kunth 1991). Stellar evolution produces a gradual change with time of the integrated stellar energy distribution, which has to be taken into account in the modeling of giant H II regions. Numerous studies have produced grids of photoionization models for H II regions considering that aspect (e.g. Terlevich & Melnick 1985; Olofsson

1989; McGaugh 1991; Cid Fernandes et al. 1992; Bernlöhr 1993; Cerviño & Mas-Hesse 1994; García-Vargas & Diaz 1994; García-Vargas et al. 1995; Stasińska & Leitherer 1996 (hereafter SL96); Bresolin et al. 1999; Dopita et al. 2000; Moy et al. 2001; Charlot & Longhetti 2001; Stasińska et al. 2001 (hereafter SSL01); Zackrisson et al. 2001). These studies used different prescriptions for the modeling of the stellar population as well as of the nebular emission. Comparisons with observations are difficult because there are at least two independent parameters that drive the emission line properties of extragalactic H II regions: age and metallicity. The general conclusion from these studies is that the Salpeter initial mass function with an upper stellar mass limit around  $100 M_{\odot}$  is consistent with the observed emission line ratios (although Bresolin et al. (1999) argue for a lower cut-off mass at high metallicity). However, several problems are noted. All the models for instantaneous starbursts predict a strong drop in [O III]  $\lambda 5007/H\beta$  at about 5 Myr. This corresponds to the maximum lifetime of O stars so the prediction is very robust. The age of a starburst in an isolated giant H II region can be estimated, to a first approximation, from the equivalent width of H $\beta$ ,  $EW(H\beta)$  (this is not feasible in giant H II re-

Send offprint requests to: G. Stasińska,  
e-mail: grazyna.stasinska@obspm.fr

gions belonging to spiral galaxies, where old stellar populations strongly contribute to the continuum at  $H\beta$ ). Using samples of isolated extragalactic H II regions, hereinafter referred to as H II galaxies, SSL01 and Zackrisson et al. (2001) showed that the observed drop was rather mild and displaced towards lower values of  $EW(H\beta)$ . SSL01 attributed this to the effect of underlying old populations of stars, shown by Raimann et al. (2000) to be present in H II galaxies. Other causes such as leakage of ionizing photons or selective dust extinction were also mentioned. The classical diagnostic diagram  $[O III] \lambda 5007/H\beta$  vs.  $[O II] \lambda 3727/H\beta$  does not seem to be completely understood in terms of pure photoionization models. One way out is to advocate some additional heating (SSL01) or the contribution of zones of low ionization parameter (Moy et al. 2001). A very significant trend of  $[O I] \lambda 6300/H\beta$  increasing with decreasing  $EW(H\beta)$ , discovered by SL96 and SSL01 remains to be quantitatively explained.

The purpose of the present paper is to quantify the conditions needed to reproduce the observed emission line sequence of giant H II regions, including the very small dispersion seen in many emission line diagrams. For a more meaningful comparison of models with observed data, our observational sample is composed of objects for which the age of the ionizing star cluster and the metallicity can be estimated in an independent way. This limits the sample to H II galaxies with measured  $[O III] \lambda 4363$  line intensities. It is only when such a sample is fully understood that one has a chance to better understand the entire extragalactic H II region sequence, including more metal-rich H II regions such as those found in the inner parts of disk galaxies.

In Sect. 2 we describe the observational sample to which we compare the models and the preliminary treatments of the data. In Sect. 3 we outline the modeling strategy, and in Sect. 4 we present our results. The main findings of our paper are summarized and discussed in Sect. 5.

## 2. The observational sample

The total sample consists of two subsamples.

Galaxies in the first subsample have been extracted mainly from the First and Second Byurakan surveys. The total number of the galaxies is  $\sim 100$ . The high signal-to-noise ratio spectra of these galaxies in the wavelength range  $\lambda 3600 - 7400\text{\AA}$  have been obtained with different 2m - 10m class telescopes. Some galaxies were observed several times. We included in the sample only one observation of each galaxy for which the spectrum was obtained with the highest signal-to-noise ratio. The spectra were reduced in a homogeneous way according to prescriptions by Izotov et al. (1994, 1997) and have been used for He and heavy element abundance determination in a series of published papers. The line intensities corrected for extinction can be found in Izotov et al. (1994, 1997, 1999, 2001a, 2001b), Izotov & Thuan (1998), Thuan et al. (1995, 1999), Lipovetsky et al. (1999), Guseva et al. (2000, 2001).

Hereafter we will call this subsample the “Byurakan sample”.

The second subsample includes  $\sim 300$  emission-line galaxies from the early data release (EDR) of the SLOAN digital sky survey (SDSS) (Stoughton et al. 2002). Hereafter we will call this subsample the “SDSS sample”. The flux-calibrated spectra of these galaxies in the wavelength range  $\sim \lambda 3820 - 9300\text{\AA}$  obtained with  $3''$  round slits have been extracted from the Space Telescope Science Institute archives<sup>1</sup>. As in the case of the Byurakan sample we included in the SDSS sample only galaxies with a detected  $[O III] \lambda 4363$  emission line. The extracted spectra have been transformed to the linear wavelength scale and zero redshift. The line intensities have been measured by Gaussian fitting to the line profiles. The errors in line intensities include the errors of Gaussian fitting and those of the continuum level. Then the line intensities have been corrected for the interstellar extinction and underlying hydrogen stellar absorption lines from the observed Balmer decrement. The emission line intensities relative to  $H\beta$  and the  $H\beta$  equivalent widths are available on request to Y. Izotov. Because the spectra in the SDSS sample start from  $\sim \lambda 3820\text{\AA}$  the line  $[O II] \lambda 3727$  has not been detected in low-redshift galaxies with  $z \lesssim 0.025$ . In those cases the intensity of the  $[O II] \lambda 3727$  emission line was calculated from the intensities of the  $[O II] \lambda 7320, 7330$  emission lines. Another problem with the SDSS spectra is that in many cases some strongest lines, most often  $H\alpha$  and  $[O III] \lambda 5007$ , are clipped. Therefore, many objects with strong emission lines were not included in our sample. However, in the cases when only  $H\alpha$  and  $[O III] \lambda 5007$  emission lines are clipped, their intensities are adopted to be respectively  $2.8 \times I(H\beta)$  and  $3 \times I([O III] \lambda 4959)$ . In general, the galaxies from the SDSS sample are fainter than those from the Byurakan sample and their spectra are of lower signal-to-noise ratio.

The main characteristics of the Byurakan and SDSS samples are compared in Fig. 1 which shows histograms of the values of redshifts  $z$  (panel a),  $H\beta$  equivalent widths  $EW(H\beta)$  (panel b), colour excesses  $E(B - V)$  as derived from the Balmer decrement (panel c) and  $H\beta$  luminosities,  $L(H\beta)$  (panel d). SDSS sample data are represented by a solid line and Byurakan sample data by a dotted line. On average, the SDSS galaxies are more distant but the  $H\beta$  luminosities are similar to those of the Byurakan sample. The equivalent width distributions are different, being more skewed toward large equivalent widths in the Byurakan sample. Note that many galaxies from the Byurakan sample have been selected for the primordial helium abundance determination, favouring large equivalent widths of the emission lines. On the other hand, since the SDSS galaxies are more distant on average, a larger fraction of galaxy light falls within the slit, contributing to the continuum at  $H\beta$ . However, we found no correlation between  $EW(H\beta)$  and redshift, which seems to indicate that statistically, the light from the underly-

<sup>1</sup> <http://archive.stsci.edu/sdss>.

ing galaxy does not contribute substantially to  $EW(H\beta)$ . The distributions of  $E(B - V)$  are roughly similar in both samples. For the majority of the objects, the extinction is small.

### 2.1. Plasma diagnostics

The electron number densities derived from  $[S II] \lambda 6731/6717$  line ratios in the objects from the Byurakan sample are small (around  $100 \text{ cm}^{-3}$  or smaller for most objects). They are more uncertain in the galaxies from the SDSS sample because of the lower signal-to-noise ratio spectra. Therefore, in the abundance determinations, a density of  $100 \text{ cm}^{-3}$  was assumed for those objects. The oxygen abundances have been obtained from the reddening corrected emission line intensities with the electron-temperature-based method. The temperature  $T_{[O III]}$  derived from  $[O III] \lambda 4363/5007$  was taken as representative of the  $[O III] \lambda 5007$  and  $H\beta$  emission, and the  $[O II] \lambda 3727$  line was assumed to be emitted at a temperature of  $0.7 \times (T_{[O III]} - 10,000 \text{ K}) + 10,000 \text{ K}$  as in SL96. The ionization correction for ionization stages higher than  $O^{++}$  is minimal. The derived oxygen abundances in our sample range between  $10^{-5}$  and  $2 \times 10^{-4}$ .

### 2.2. Comparison to former samples

Our merged sample is far more numerous than the Izotov or Popescu & Hopp (2000) samples used in SSL01, since it contains around 400 objects. It is of comparable size to the entire sample of H II galaxies from the Terlevich et al. (1991) survey, which comprised about 300 objects. However, being limited to objects with low metallicities and  $EW(H\beta)$  larger than  $10\text{\AA}$  due to the condition imposed on the detection of  $[O III] \lambda 4363$ , our sample is four times more numerous than the Terlevich sample per bin of metallicity and equivalent width. In addition, the signal-to-noise ratio in our sample is generally much higher than in the Terlevich sample. This gives us the opportunity to investigate the evolution of H II galaxies using statistical considerations with unprecedented detail.

### 2.3. Observational trends

Figure 2 presents our entire sample of H II galaxies in a set of diagrams involving emission line ratios and  $EW(H\beta)$ . The number of data points present in each diagram is shown in the upper right of each panel. The trends noted in SSL01 are clearly confirmed. Most conspicuous are the decrease of  $[O III] \lambda 5007/[O II] \lambda 3727$  and the increase of  $[O I] \lambda 6300/([O II] \lambda 3727 + [O III] \lambda 5007)$  as  $EW(H\beta)$  decreases, as well as the constancy of  $He I \lambda 5876/H\beta$  and  $([O II] \lambda 3727 + [O III] \lambda 5007)/H\beta$  and the mild decrease of  $[O III] \lambda 5007/H\beta$ . There is also a clear tendency for  $[N II] \lambda 6584/[O II] \lambda 3727$  to increase as  $EW(H\beta)$  decreases, although the relation is more dispersed. The pure emission line diagnostic diagrams  $[O III] \lambda 5007/H\beta$  vs.

$[O II] \lambda 3727/H\beta$  and  $[O III] \lambda 5007/H\beta$  vs.  $[O I] \lambda 6300/H\beta$  do not draw such an extended sequence as when using data including objects with higher metallicities, such as H II regions located in the central parts of spiral galaxies (McCall et al. 1985; van Zee et al. 1998a), but the points are strongly gathered in a well defined zone of the plane. When plotting the Byurakan sample and the SDSS sample separately, the points are indistinguishable in these diagrams in the zone of overlap of  $EW(H\beta)$ , except that the  $He I \lambda 5876/H\beta$  shows much less scatter due to the higher quality of the data. This indicates that the nature of the objects is similar and justifies the merging of the two samples for the study of the emission line sequence in H II galaxies.

In the  $He II \lambda 4686/H\beta$  vs.  $EW(H\beta)$  diagram, the number of points is much smaller than in the previous diagrams. The reason is not only that  $He II \lambda 4686$  is a weak line, but also that this line is difficult to measure since it is superimposed on the Wolf-Rayet bump seen in the spectra of many H II galaxies (Guseva et al. 2000). It could not be extracted in the fainter objects from the SDSS sample because of the lower signal-to-noise ratio in their spectra, and could be safely measured only in 48 objects from the Byurakan sample. The lower envelope is obviously an observational effect. What is important to note is that the dispersion is rather large, that nebular  $He II \lambda 4686$  line is detected in the entire range of  $EW(H\beta)$  of our sample, and that no tendency is seen with  $EW(H\beta)$  (see also Guseva et al. 2000).

The fact that a sample of 400 objects shows such a conspicuous collective behaviour in the plots of Fig. 2 is remarkable, given that detailed studies of a few of them show that their nature is rather complex (Thuan et al. 1997, 1999; Papaderos et al. 1998, 1999; Stasińska & Schaerer 1999). This means that, in spite of this complexity, the evolution of H II galaxies obeys simple laws. In the following, we will aim at describing this evolution in an empirical way using photoionization models, in order to find some clues on the driving mechanisms of this evolution.

## 3. Modeling

### 3.1. The modeling codes

The computations are done with the same codes as used by SSL01. The theoretical spectral energy distributions are obtained from the evolutionary synthesis models of Schaerer & Vacca (1998)<sup>2</sup>. They use the non-rotating Geneva stellar evolution models, with the high mass-loss tracks of Meynet et al. (1994). The spectral energy distributions for massive main-sequence stars are taken from the *CoStar* models (Schaerer & de Koter 1997), which include the effects of stellar winds, non-LTE, and line blanketing in an approximate manner. The pure He models of Schmutz et al. (1992) are used for Wolf-Rayet stars. The spectral energy distributions from the plane-parallel LTE

<sup>2</sup> The predictions from these synthesis models are available on the Web at <http://webast.ast.obs-mip.fr/people/schaerer/>.

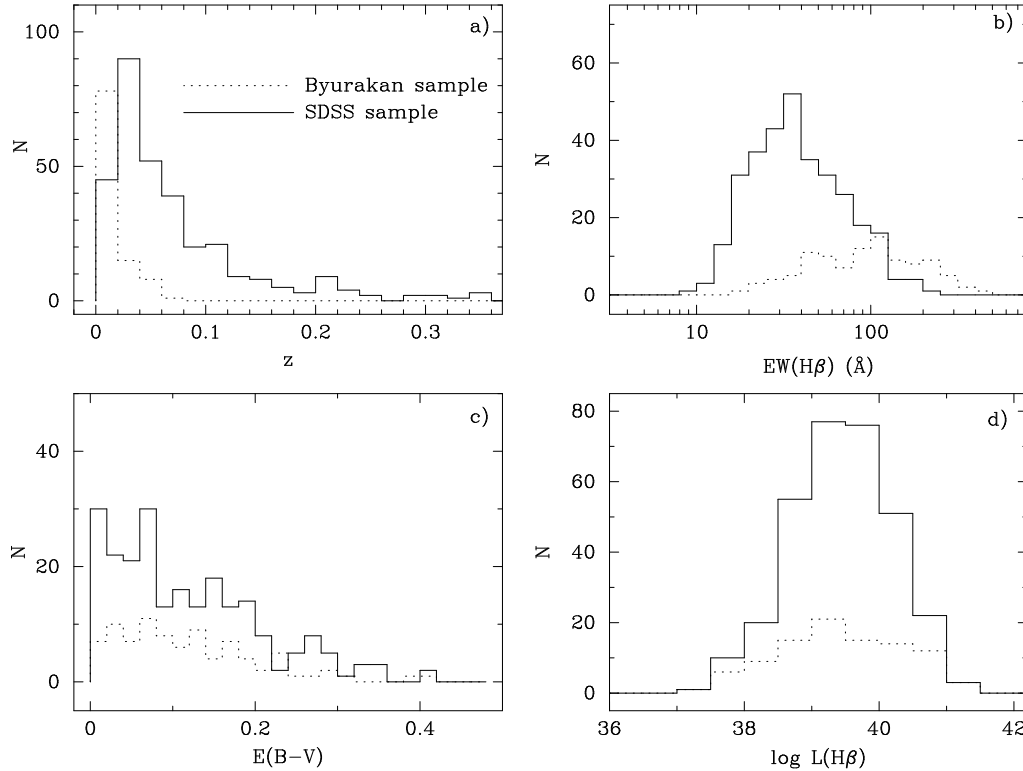


**Fig. 1.** Histograms of redshifts  $z$  (panel a),  $H\beta$  equivalent widths (panel b), colour excesses  $E(B - V)$  as derived from the Balmer decrement (panel c) and  $H\beta$  luminosities (panel d). SDSS sample data are represented by a solid line and Byurakan sample data by a dotted line.

models of Kurucz (1991) are used for the low mass stars which build up the continuum.

Recent computations of stellar energy distributions using more complete stellar atmosphere codes (Hillier & Miller 1998; Pauldrach et al. 2001) show significant differences with the models used in the present work. The most important differences, however, concern high metallicity stars. At the metallicities relevant for our studies, the agreement with the atmospheres used here is reasonable. In general, the ionizing radiation predicted by the new model atmospheres is softer than that predicted by the model atmospheres entering the population synthesis of Schaerer & Vacca (1998). This concerns both the main sequence O-stars (resulting in a smaller ratio of  $He^0$  to  $H^0$  ionizing photons  $Q_{He^0}/Q_H$ ) and Wolf-Rayet stars (resulting in a smaller  $Q_{He^+}/Q_H$ ). Stellar population synthesis models including these new atmosphere models were not yet available at the time when the present work was done. But they are not expected to significantly alter the conclusions of the present work.

The photoionization models using the spectral energy distributions as an input are built with the code PHOTO, as described in SL96.

### 3.2. The modeling strategy

Instead of producing wide grids of models, as in the studies listed in the introduction, we try to fit the observed

data with sequences of models that would represent the true evolution of a giant H II region excited by a cluster of evolving stars. We take advantage of the fact that we have determined the oxygen abundance (hereafter simply referred to as the metallicity) for all the objects of our sample, so that each object can be compared to one model of given metallicity. To make the problem visually tractable, we divide our sample of objects in three metallicity bins: the “high” metallicity bin contains all the objects of our sample having  $O/H > 10^{-4}$  (i.e. larger than 0.12 times the solar oxygen abundance as given by Anders & Grevesse 1989), the “intermediate” one contains all the objects with  $O/H$  between  $10^{-4}$  and  $3 \times 10^{-5}$  (i.e. between 0.12 and 0.036 times solar) and the “low” metallicity bin contains all the objects with  $O/H < 3 \times 10^{-5}$  (i.e. less than 0.036 times solar). Obviously, the words “high”, “intermediate” and “low” are not to be taken literally in this context, since our entire sample is composed of objects with  $O/H < 2 \times 10^{-4}$  (i.e. less than 0.25 times the solar value). We have not included in any metallicity bin the objects (from the SDSS data) for which the estimated error in the  $[O III] \lambda 4363$  intensity is larger than 50% in order to limit undue shift of metallicity bins as a consequence of important errors in the abundance determinations. Each metallicity bin is compared to models with corresponding metallicity:  $Z = 0.2 Z_\odot$ ,  $Z = 0.05 Z_\odot$ , and  $Z = 0.02 Z_\odot$ , for the “high”, “intermediate” and “low” metallicity bins respectively. As in SSL01 and in most recent studies on

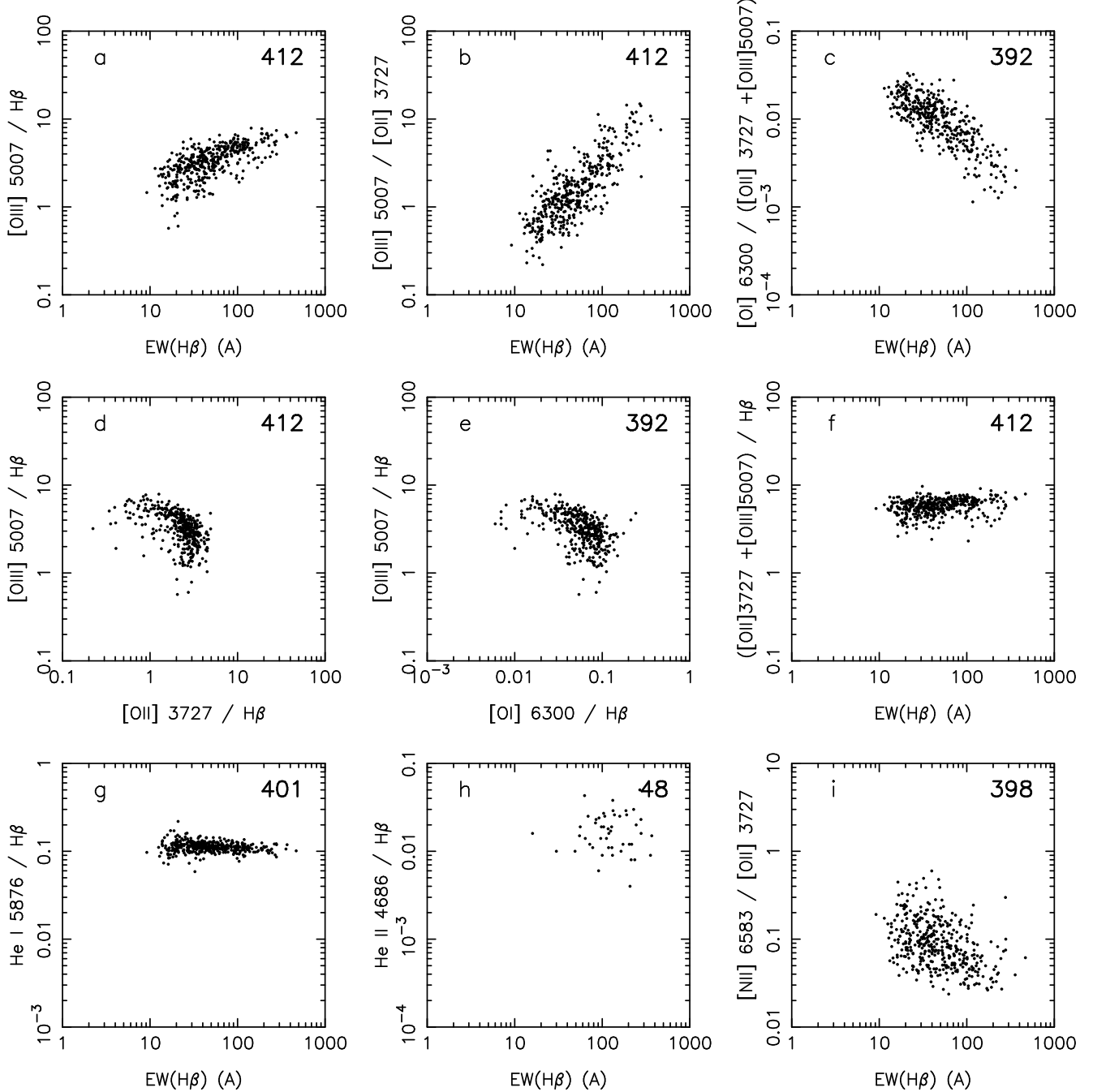


**Fig. 2.** The entire sample of H II galaxies in a set of diagrams involving emission line ratios and  $EW(H\beta)$ . The number of data points present in each diagram is shown in the upper right of each panel.

extragalactic H II regions, we adopt as a reference the solar abundances from Anders & Grevesse (1989), although the latest determinations of solar abundances are significantly different. Especially, the oxygen abundance in the Sun as derived by Allende Prieto et al. (2001) is  $4.9 \times 10^{-4}$  instead of  $8.5 \times 10^{-4}$  by Anders & Grevesse (1989). In the present work, the term “solar” is used for an easier reference with previous work. As in SSL01, we use the McGaugh (1991) prescription to link the abundances of all the elements to the abundance of oxygen. In particular,  $He/H = 0.0772 + 15 (O/H)$  and  $\log N/O = 0.5 \log (O/H) + 0.4$ .

In all cases, we use for the ionizing star cluster a Salpeter initial mass function with an upper mass limit of  $120 M_{\odot}$  and a lower mass limit of  $0.8 M_{\odot}$ , and we assume an instantaneous burst. Sequences of models are built with ages spaced by time intervals of 0.5 Myr starting from 0.01 Myr. Unless expressed explicitly, the metallicity of the nebula is the same as that of the ionizing cluster, and the ionized gas contains no dust.

Our aim is to reproduce the observational diagrams as well as possible, with the simplest physically reasonable models.

The first step is to model the H II regions not as static gaseous spheres or thin bubbles with constant radius as was done in all the previous works mentioned in the introduction, but to explicitly take into account the expected time variation of the gas density distribution. As a simple representation, we chose the model of supernova/wind driven bubble in an adiabatic phase, which consists of a thin spherical shell of density  $n$  and radius given by the expression  $R = At^{3/5}$  cm, where  $t$  is the age in Myr. Such an approach has already been used in the past for a detailed modeling of several giant H II regions, in which the observed size was also used as a constraint (García-Vargas et al. 1997; Maíz-Apellániz et al. 1999). In the case of constant mechanical energy, the value of  $A$  is linked to the energy injection  $\dot{E}$  and to the density  $n_0$  of the ambient medium by  $A = 5.1 \times 10^{12} (\dot{E}/n_0)^{1/5}$  (Weaver et al. 1977). By trial and error, we take  $A = 2 \times 10^{20}$  cm which, for a typical value of  $n_0 \simeq 1 \text{ cm}^{-3}$  (see e. g. van Zee et al. 1998b) corresponds to  $\dot{E} \simeq 9 \times 10^{37} \text{ erg s}^{-1}$ . Note that, for the stellar population synthesis models we use, the mechanical luminosity from stellar winds and supernovae during the first 3 Myr of a burst with initial mass of  $10^5 M_\odot$  is estimated to be  $\sim 2 \times 10^{38} \text{ erg s}^{-1}$  at  $0.2 Z_\odot$  and  $5 \times 10^{37} \text{ erg s}^{-1}$  at  $0.05 Z_\odot$  (Leitherer et al. 1999). The models are built with a density  $n = 100 \text{ cm}^{-3}$ . The integrated initial mass of the stellar population,  $M_*$ , is taken to be  $10^5 M_\odot$ , which corresponds to a total H $\beta$  luminosity of  $3.5 \times 10^{39} \text{ erg s}^{-1}$  at an age of 1 Myr if all the ionizing photons are converted into Balmer line photons under case B. Note that results from photoionization models (line ratios and H $\beta$  equivalent width) remain identical to the ones presented here for other values of  $M_*$  if  $R$  is changed accordingly (i.e. multiplied by  $(M_*/10^5 M_\odot)^{0.5}$  so that the ionization parameter  $U = Q_H/(4\pi R^2 nc)$  is conserved).

Starting from this simple expanding bubble model, we proceed by modifying the model assumptions step by step, until the theoretical sequences match all the observed diagrams satisfactorily. Note that, at an age of 0.01 Myr, our parametrisation implies a bubble radius of about 4 pc, which is the typical size of a stellar cluster. It can easily be shown that, for such a situation, our models will overestimate the ionization parameter since they assume that all the stars are located at the center of the bubble, while the real situation is closer to that of a cluster of Strömgren spheres.

In the forthcoming figures, the models pertaining to a given evolutionary sequence are represented by the same symbol, and two consecutive models are linked with a straight line. Since the models are built at equally spaced time intervals, the distribution of observational points in a diagram should approximately follow the distribution of the symbols. Models having  $[\text{O III}] \lambda 4363/\text{H}\beta < 2 \times 10^{-2}$ , which roughly corresponds to the lower limit of the intensities of the  $[\text{O III}] \lambda 4363$  line in our sample, are represented by small symbols. Table 1 summarizes the main characteristics of the models shown in the figures.

**Table 1.** Description of the model sequences

name	$Z_*$	$Z_{neb}$	old stars	$a f$	X-rays
H1	0.2	0.2	no	1	no
H2	0.2	0.2	yes	1	no
H3	0.2	0.2	yes	$0.5 \exp(-t/3)$	no
I1	0.05	0.05	no	1	no
I2	0.05	0.05	yes	1	no
I3	0.05	0.05	yes	$0.5 \exp(-t/3)$	no
I4	0.05	0.05	yes	$0.5 \exp(-t/3)$	yes
I5	0.05	0.2	yes	$0.5 \exp(-t/3)$	yes
L4	0.02	0.02	yes	$0.5 \exp(-t/3)$	yes
L5	0.02	0.2	yes	$0.5 \exp(-t/3)$	yes

## 4. Results

### 4.1. The “high” metallicity bin

Figure 3 shows, in the same diagrams as Fig. 2, our “high” metallicity subsample, which is composed of 105 objects. Overplotted with circles is the starting sequence of models, with metallicity  $Z = 0.2 Z_\odot$  and  $A = 2 \times 10^{20}$  cm (sequence H1). This sequence of models reproduces the classical emission line ratio diagrams  $[\text{O III}] \lambda 5007/\text{H}\beta$  vs.  $[\text{O II}] \lambda 3727/\text{H}\beta$  and  $[\text{O III}] \lambda 5007/\text{H}\beta$  vs.  $[\text{O I}] \lambda 6300/\text{H}\beta$  (panels d and e) reasonably well. It also reproduces the tendency for  $[\text{O I}] \lambda 6300/\text{H}\beta$  to increase as  $EW(\text{H}\beta)$  decreases (panel c) due to the fact that, in the expanding bubble scenario, the ionization parameter strongly decreases with time (while in the static models considered in the previous studies, it decreases only because of the gradual disappearance of the most massive stars). In this scenario, there is no difficulty in reaching the highest  $[\text{O I}] \lambda 6300/\text{H}\beta$  observed. However, this sequence of models does not reproduce the slope of the observational points in the  $[\text{O I}] \lambda 6300/\text{H}\beta$  vs.  $EW(\text{H}\beta)$  diagram. More importantly, it does a very bad job for the  $[\text{O III}] \lambda 5007/\text{H}\beta$  vs.  $EW(\text{H}\beta)$ ,  $[\text{O III}] \lambda 5007/[\text{O II}] \lambda 3727$  vs.  $EW(\text{H}\beta)$ , and  $\text{He I } \lambda 5876/\text{H}\beta$  vs.  $EW(\text{H}\beta)$  diagrams (panels a, b and g, respectively). As stated in SSL01, most H II galaxies are likely to contain stars from previous star forming episodes which do not contribute to the H $\beta$  flux and reduce the value of  $EW(\text{H}\beta)$  with respect to a pure starburst model. Such populations of older stars (hereinafter referred to as old populations for simplicity) have been directly inferred from deep CCD images (Loose & Thuan 1985; Papaderos et al. 1996) and from weak stellar features detected in the continuum (e.g., Kong & Cheng 1999; Mas-Hesse & Kunth 1999; Raimann et al. 2000; Guseva et al. 2001). Statistically, the total flux in the continuum arising from old stellar populations should not depend on the age of the most recent burst of star formation which provides the ionizing stars of the H II regions. For an illustration, we show in Fig. 3 as squares the locations of the same model sequence as our starting one but with an old population whose continuum at H $\beta$  is equal to the stellar continuum

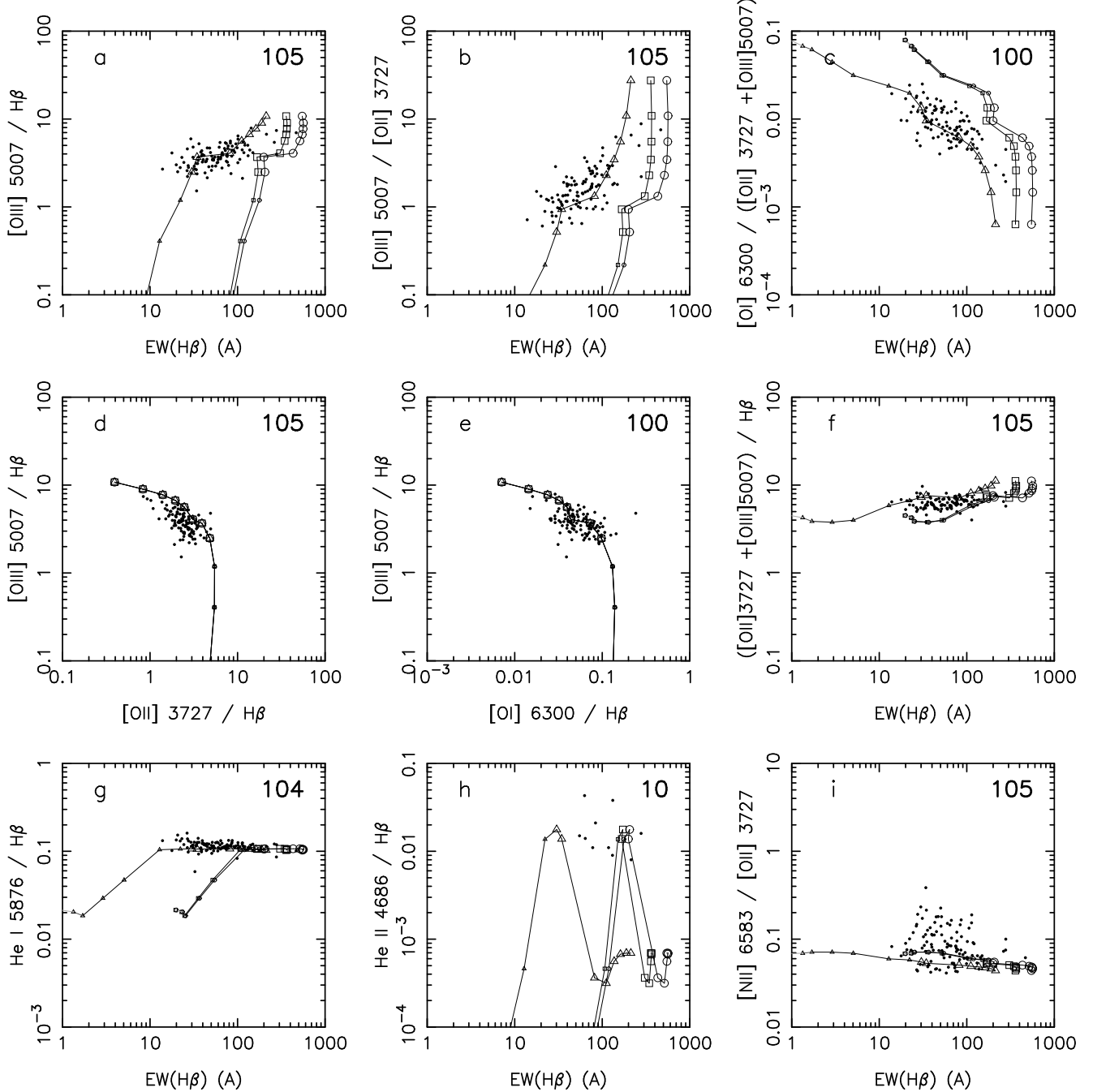


**Fig. 3.** The “high” metallicity bin. The data points correspond to the objects of our sample for which the estimated error in the [O III]  $\lambda$ 4363 intensity is less than 50% and which have O/H  $> 10^{-4}$ . The number of data points present in each diagram is shown in the upper right of each panel. Overplotted are evolutionary sequences of models with metallicity  $Z = 0.2 Z_{\odot}$ . For each sequence, symbols are plotted at time intervals of 0.5 Myr. Small size symbols correspond to models having [O III]  $\lambda$ 4363/H $\beta$   $< 2 \times 10^{-2}$ , which roughly corresponds to the lower limit of the intensities of the [O III]  $\lambda$ 4363 line in our sample. The sequence represented with circles corresponds to the expanding bubble model H1 (for complete descriptions of the model sequences, see text and Table 1). The sequence represented with squares corresponds to model H2 (i. e. same as H1 but with an underlying older population). The sequence represented with triangles corresponds to model H3 (i. e. same as H2 but with a varying covering factor).

from the most recent starburst at the age of 0.01 Myr (sequence H2). Such a small value seems appropriate for our objects since the observed spectral energy distributions (SED) of young star forming regions in some galaxies from

the Byurakan sample can be fitted by the theoretical SEDs with large fraction of the light from the 3 – 5 Myr old stellar populations and minor contribution of the older non ionizing populations (e.g. Papaderos et al. 1998; Thuan

et al. 1999; Guseva et al. 2001). This brings the values of  $EW(H\beta)$  for the earliest stages in closer agreement with the maximum observed values. However, this still does not reproduce the slopes defined by the observational points in the  $[O III] \lambda 5007/H\beta$  vs.  $EW(H\beta)$  and  $[O III] \lambda 5007/[O II] \lambda 3727$  vs.  $EW(H\beta)$  diagrams (panels a and b) and the fact that  $He I \lambda 5876/H\beta$  is observed to be constant down to  $EW(H\beta)$  as small as 10. Choosing a larger contribution of the underlying population does not help to explain the behaviour of the observational points in panels a, b and c. Other effects have been invoked in the literature that may reduce  $EW(H\beta)$ . One of them is the fact that in starburst galaxies, the nebular lines seem to come from dustier regions than the stellar continuum (Calzetti et al. 1994, Gordon et al. 1997). However, in our sample, the nebular extinction is generally very small (see Fig. 1c) so that the effect, if existing, will be negligible for the vast majority of our objects. Similarly, assuming that a typical aperture correction  $a$  should be applied to the models will roughly translate the curves towards the left, but will not much affect the slope in these diagrams. What is needed is to obtain models in which  $EW(H\beta)$  decreases with time more rapidly, without affecting the  $[O III] \lambda 5007/H\beta$  or  $[O III] \lambda 5007/[O II] \lambda 3727$  ratios. This can be achieved by assuming that the covering factor  $f$  decreases with time, so that an increasing fraction of ionizing photons is not processed into  $H\beta$ . Such a scenario is not unlikely, since the true geometry may not be spherical but rather axisymmetrical. Then, during late stages, the matter from the polar directions will have been blown out at high velocities, and the matter giving rise to the bulk of the emission would rather have the form of a ring. This is indeed the geometry suggested from the  $H\alpha$  map of I Zw 18 (Stasińska & Schaerer 1999). Another way to obtain a covering factor decreasing with time is in the case of gradual clumping due to instabilities. To make things simple, we assume that time dependence of the covering factor is exponential. By trial and error, we find that  $f = \exp(-t/3)$ , where  $t$  is the time expressed in Myr, provides a reasonable fit to the observed data in panels a, b, c and g, if we maintain the contribution of the old stellar population as in the sequence represented with squares and if we assume an aperture correction  $a=0.5$ . This is likely a conservative estimate of the aperture correction in our sample. For the closest objects, the  $H\alpha$  emission is more extended than the part entering the slit. Therefore,  $EW(H\beta)$  as measured from spectra is smaller than computed by models. Guseva et al. (2000) have determined the aperture correction for 33 galaxies from the Byurakan sample and found a mean value of 0.33. For distant objects, the slit includes the entire H II region and also an extended old population of stars from the underlying galaxy, if present. However, as noted in Sect. 2, the fact that there is no correlation between redshift and  $EW(H\beta)$  suggests that, statistically, the contribution of the old population to the  $H\beta$  continuum is not very large. The resulting sequence is represented by triangles in Fig. 3 (sequence H3). This sequence also reproduces the  $([O II] \lambda 3727 + [O III] \lambda 5007)/H\beta$  vs.

$EW(H\beta)$  diagram. Of course, the inclusion of an old stellar population and of a decreasing covering factor does not change the location of the model points in the line-ratio diagnostic diagrams (panels d and e).

Therefore, we reach the conclusion that the scenario of an adiabatically expanding bubble ionized by a coeval cluster of stars reproduces both the line ratio diagrams and the evolutionary diagrams remarkably well, provided that account is taken for an old stellar population and for a covering factor decreasing with time.

The dispersion of the observational points in Fig. 3 is perfectly accounted for (within two sigmas) if the value of  $A$  defining the radius of the bubble lies within  $\pm 0.3$  dex of the value adopted for the models shown in the figure.

We note that the  $He II \lambda 4686/H\beta$  vs.  $EW(H\beta)$  diagram is however not well reproduced by such a sequence. Indeed,  $He II \lambda 4686$  lines are observed at equivalent widths between 300 and 50 Å in our “high” metallicity subsample, while the models predict  $He II \lambda 4686$  line intensities at the level of 0.01 of  $H\beta$  only at  $EW(H\beta)$  around 30 Å, when Wolf-Rayet stars are present. Of course, this value of  $EW(H\beta)$  at which Wolf-Rayet stars appear is dependent on the underlying stellar population and the covering factor, so that some dispersion is allowed. However, one does not expect more than 25 – 35 % of cases with  $He II \lambda 4686/H\beta$  of the order of 0.01. Our subsample contains 10 such objects out of 28 in which the quality of the data is sufficient to detect the  $He II \lambda 4686$  line if it were present. Of course, one can argue that we are dealing with small number statistics and that statistical effects are particularly important when considering the  $He II \lambda 4686$  lines which are produced by only a small fraction of stars (Cerviño et al. 2000). The problem will be clearer when considering the next subsamples.

Also, our models do not reproduce the observed tendency of  $[N II] \lambda 6584/[O II] \lambda 3727$  to increase as  $EW(H\beta)$  decreases. We will come back to this below. For the moment, let us simply note that our former conclusions are not affected by this failure.

#### 4.2. The “intermediate” metallicity bin

Figure 4 shows the same diagnostic diagrams as Fig. 3 for our “intermediate” metallicity subsample, which contains 171 objects. Overplotted with circles, squares and triangles are the model sequences I1, I2, I3. These sequences are identical to sequences H1, H2, H3 respectively except for the metallicity which is  $Z = 0.05 Z_{\odot}$ , relevant to this subsample. We immediately see that the models reproduce the observational sequence much less satisfactorily than in the “high” metallicity bin. Clearly, no solution can be found by simply changing the value of  $A$  in the expression giving the radius of the bubble, the contribution of the underlying old population or the law of variation of the covering factor. Whatever solution which would increase the  $[O I] \lambda 6300/H\beta$  ratio and bring it in better agreement with the observations would simultaneously decrease the



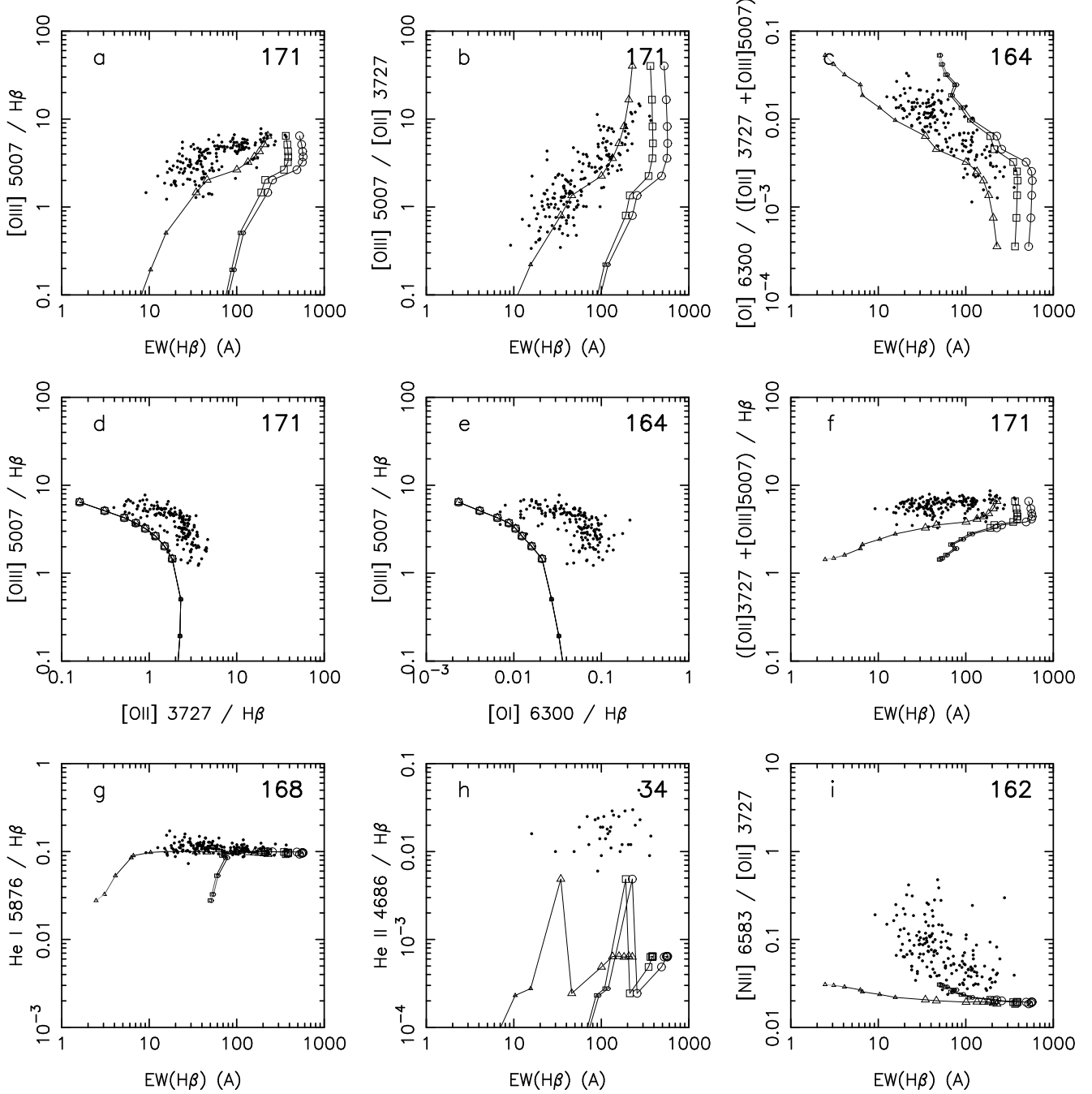


**Fig. 4.** Same as Fig. 3, for the “intermediate” metallicity bin. The data points have  $3 \times 10^{-5} < \text{O}/\text{H} < 10^{-4}$ . The models are constructed with metallicity  $Z = 0.05 Z_{\odot}$ . The sequences of models represented by circles, squares and triangles correspond to model sequences I1, I2 and I3 respectively (for complete descriptions of the model sequences, see text and Table 1).

[O III]  $\lambda 5007/\text{H}\beta$  ratio and make the situation worse in the [O III]  $\lambda 5007/\text{H}\beta$  vs.  $\text{EW}(\text{H}\beta)$  diagram. The model sequences are significantly displaced to the lower left of the observed sequences in the [O III]  $\lambda 5007/\text{H}\beta$  vs. [O II]  $\lambda 3727/\text{H}\beta$  and [O III]  $\lambda 5007/\text{H}\beta$  vs. [O I]  $\lambda 6300/\text{H}\beta$  diagrams (panels d and e) and below the ([O II]  $\lambda 3727 + [\text{O III}] \lambda 5007)/\text{H}\beta$  zone (panel f). One way to propose a diagnostic is to say that there is not enough heating in the models, so that the ratios of collisionally excited to re-

combination lines are too small. We have attempted to remedy this situation by a variety of means. For example, we have considered depletion of metals into dust grains, as well as heating by photoelectric effect on small grains using the prescriptions described in Stasińska & Szczerba (2001): this is by far insufficient, given that the dust-to-gas mass ratio cannot exceed the maximum available mass of elements that can be condensed into grains, and that the ionization parameter is very low ( $U = 10^{-2}$  at  $t =$

1 Myr,  $U = 4 \times 10^{-4}$  at  $t = 4$  Myr). An inhomogeneous density distribution does not help either. Obviously, one cannot charge the Costar or the Schmutz et al. (1992) model atmospheres used for the spectral energy distribution in our models, since they precisely give harder fluxes than the more accurate model atmospheres of Pauldrach et al. (2001) or Hillier & Miller (1998).

One clue might come from the He II  $\lambda 4686/H\beta$  diagram. Using the models described above, we predict that He II  $\lambda 4686$  should be measurable (He II  $\lambda 4686/H\beta \sim 0.01$ ) in less than 20% of objects, (the time resolution of our computations actually makes us miss the highest He II  $\lambda 4686/H\beta$  value), corresponding to the lifetime of massive Wolf-Rayet stars. However, in the Byurakan “intermediate” metallicity subsample there are 34 objects out of 62 with He II  $\lambda 4686/H\beta$  at the level of 0.01. Therefore, the statistical fluctuation argument cannot be invoked here. Nuclei of planetary nebulae and hot dwarfs born in previous episodes of star formation are not expected to provide sufficient ionizing photons to significantly increase the He II  $\lambda 4686/H\beta$  ratio. Cerviño (2000) and Cerviño et al. (2002) have invoked X-rays to produce the He II  $\lambda 4686$  line in giant H II regions. Such X-rays can be produced by a variety of sources: individual stars (their contribution is in fact considered negligible by these authors), binary stars, supernova remnants and hot diffuse gas. In the evolutionary population synthesis models of Cerviño et al. (2002), the X-ray production is estimated as a function of an efficiency conversion factor from the mechanical kinetic energy injection from stellar winds and supernova explosions into X-ray radiation. From their study, assuming an efficiency conversion factor of 20%, the amount of X-ray energy released by a cluster of metallicity  $0.05 Z_{\odot}$  and initial mass of  $10^5 M_{\odot}$  goes from less than  $10^{38} \text{ erg s}^{-1}$  to a maximum of  $10^{39} \text{ erg s}^{-1}$ , which occurs at an age of around 3.5 Myr. This is far from sufficient to reproduce the observed He II  $\lambda 4686/H\beta$  ratios, which range between 0.01 and 0.03 for any value of  $EW(H\beta)$  below  $300 \text{ \AA}$ . Assuming that the He II  $\lambda 4686$  emission is more concentrated than the  $H\beta$  one and taking into account that the slit does not cover the entire H II region will shift the observational points downwards by a factor about 2 (Guseva et al. 2000). This is not enough to put into agreement observations and model predictions.

We have constructed a sequence of models with the same characteristics as the one presented in Fig. 4 but with an additional source of X-rays, radiating as bremsstrahlung at a temperature of  $10^6 \text{ K}$  and having a total luminosity of  $4 \times 10^{40} \text{ erg s}^{-1}$ . This sequence of models is shown in Fig. 5 with circles (sequence I4), overplotted on the observational data similarly to Fig. 4 (we adopt the same contribution of an old population and the same law for the covering factor  $f$  as previously). From the figure, we see that such a luminosity is required to reproduce the upper envelope of the observational points. Note that these X-rays have little incidence on the other line ratios, even on  $[O I] \lambda 6300/H\beta$  which is enhanced by a factor 2 at most in the zone of interest, as can be seen by compar-

ing Figs. 4 and 5. From the range of observed values of He II  $\lambda 4686/H\beta$  we conclude that if these ratios are to be explained by photoionization due to the radiation from a thermal plasma at around  $10^6 \text{ K}$ , the total required X-ray luminosity is  $10^{40} - 4 \times 10^{40} \text{ erg s}^{-1}$  for at least half of the sources. In any case, we note that photons from such an additional X-ray source do not heat the gas strongly enough to bring models into agreement with observations in the  $[O III] \lambda 5007/H\beta$  vs.  $[O II] \lambda 3727/H\beta$  and  $[O III] \lambda 5007/H\beta$  vs.  $[O I] \lambda 6300/H\beta$  diagrams (panels d and e).

A popular way to explain discrepancies between photoionization models and observed line intensity ratios in H II regions (essentially the occurrence of high  $[O I] \lambda 6300/H\beta$  or  $[S II] \lambda 6716, \lambda 6731/H\beta$ ), is to invoke shocks. However, we note that, here, the  $[O I] \lambda 6300$  line intensities are entirely explained by pure photoionization models of reasonable geometry (the same can be said for  $[S II] \lambda 6716, \lambda 6731$  lines). As a matter of fact, the large  $[O I] \lambda 6300/H\beta$  or  $[S II] \lambda 6716, \lambda 6731/H\beta$  ratios in shocks are mainly due to photoionization from X-rays produced behind the shock front. Shocks can also heat the gas, and are sometimes invoked to explain the  $[O III] \lambda 4363/[O III] \lambda 5007$  ratios observed to be higher than obtained in tailored photoionization models of H II regions. They could then perhaps also explain the  $[O III] \lambda 5007/H\beta$  vs.  $[O II] \lambda 3727/H\beta$  diagram, by boosting the collisionally excited lines. The mechanical energy from stellar winds and supernovae from the latest burst of star formation is actually insufficient to affect appreciably the luminosities of the  $[O III] \lambda 5007$  and  $[O II] \lambda 3727$  lines, but one could argue that kinetic energy is available from previous bursts or from cloud-cloud collisions. However, it is important to note that what appears as a heating problem may actually have a completely different origin. For example, Stasińska (1999) and Moy et al. (2001) have shown that composite models including a diffuse component can displace to the left the location of model sequences in  $[O III] \lambda 5007/H\beta$  vs.  $[O II] \lambda 3727/H\beta$  or  $[O III] \lambda 5007/H\beta$  vs.  $[O I] \lambda 6300/H\beta$  diagrams without the need of any additional heating. Chemical inhomogeneities can be another appealing explanation. Take for example the same sequence of models as shown in Fig. 5 by circles, but assume that the metallicity of the gas is  $Z_{neb} = 0.2 Z_{\odot}$  (sequence I5), not  $0.05 Z_{\odot}$ . Then, combine these two sequences of models, so as to reproduce an H II region which would consist of parcels of gas with composition identical to the initial composition of the ionizing stars, and of blobs of enriched matter. Such a sequence of models is shown in squares in Fig. 5 (here, we have assumed that the relative weight of the high metallicity component with respect to the low metallicity one, in terms of  $H\beta$  luminosity, is given by the expression  $\exp(-0.5/t)$  where  $t$  is the time in Myr). The  $[O III] \lambda 5007/H\beta$  vs.  $[O II] \lambda 3727/H\beta$  and  $[O III] \lambda 5007/H\beta$  vs.  $[O I] \lambda 6300/H\beta$  diagrams (panels d and e) are now quite well reproduced. This is also the case for the  $([O II] \lambda 3727 + [O III] \lambda 5007)/H\beta$  diagram vs.  $EW(H\beta)$  diagram (panel f). This is encouraging, since  $([O II] \lambda 3727 + [O III] \lambda 5007)/H\beta$  is a first order indicator of the total energy released in the colli-

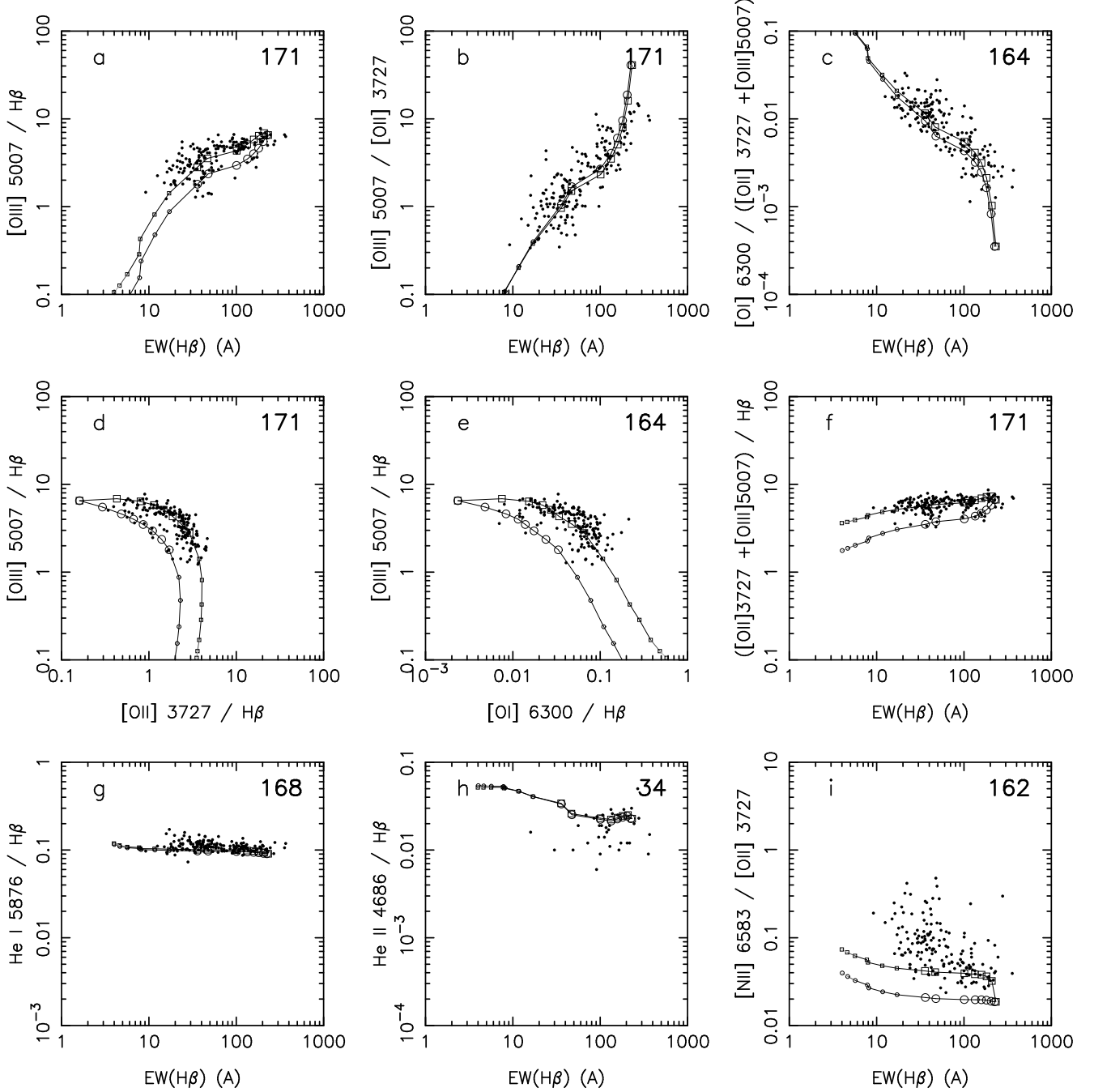


**Fig. 5.** The data points correspond to the “intermediate” metallicity bin as in Fig. 4. The model sequence represented by circles corresponds to sequence I4: expanding bubble with varying covering factor and old underlying population included, and additional ionization by X-rays. The model sequence represented by squares corresponds to the composite sequence I5, i.e. same as I4 but including the effect of self-enrichment (for complete descriptions of the model sequences, see text and Table 1).

sionally excited lines, and the basis of abundance determinations using strong lines only (see Pilyugin (2000) and references therein). Of course, we do not mean to say that this precise combined model corresponds to reality. There are many combinations that can provide an acceptable solution from the point of view of line ratios. One must be aware that, in such a hypothesis, the abundances derived by classical methods only represent some average

abundance, and there is a bias which depends on the exact abundance pattern (and perhaps also on the density pattern). A future work would be to pinpoint which solutions could be compatible with the theory of production and mixing of elements in dwarf galaxies. A more straightforward evidence for self-enrichment of the gas in H II galaxies comes from the  $[\text{N II}] \lambda 6584 / [\text{O II}] \lambda 3727$  vs.  $EW(\text{H}\beta)$  diagram (panel i). SSL01 already invoked

the possibility of self-enrichment in nitrogen from the behaviour of H II galaxies in such a diagram, irrespective of their metallicity. However, they also made the point that a similar behaviour could arise from a contribution of old stellar populations increasing with metallicity. In all the figures of the present paper (except Fig. 2) the objects are grouped by metallicity, and the trend of  $[\text{N II}] \lambda 6584 / [\text{O II}] \lambda 3727$  increasing with decreasing  $EW(\text{H}\beta)$  remains. It is even more conspicuous in the intermediate metallicity bin than in the high metallicity bin (which, remember, concerns only objects with  $\text{O}/\text{H} < 2 \times 10^{-4}$ , i.e. much smaller than the solar value).

#### 4.3. The “low” metallicity bin

Only a small proportion of objects from our sample have  $\text{O}/\text{H}$  determined to be smaller than  $3 \times 10^{-5}$ : 15 in total. Indeed, it is a known fact (e.g., Terlevich et al. 1991; Masegosa et al. 1994; Kunth & Östlin 2000) that H II galaxies with metallicities smaller than 1/25 solar are very rare. Therefore, the trends in observational diagrams are less clearly seen than in the case of the higher metallicity bins. Nevertheless, by comparing the location of the observational points in Fig. 6 with those of Fig. 5, we note that the same trends are present. Superimposed on the data points, we represent with circles the model sequence L4, which is identical to the model sequence I4 except for the metallicity which is  $Z_{\text{neb}} = Z_* = 0.02 Z_{\odot}$  instead of  $0.05 Z_{\odot}$ . We see that this sequence is a good first approximation to the observed trends (as was the case with sequence I4 for the intermediate metallicity bin). But, similarly to the intermediate metallicity bin, the predicted intensities of collisional lines with respect to  $\text{H}\beta$  are lower than observed. The problems seems even exacerbated: compare the position of the circles with respect to the data points in Figs. 6 and 5. This can be qualitatively understood if self-pollution is indeed the explanation: the effects of self-pollution are expected to be larger for lower initial metallicities. For an illustration, we plot with squares a composite model sequence similar to the one plotted in Fig. 5, except that  $Z_{\text{neb}}$  is  $0.02 Z_{\odot}$  and  $0.2 Z_{\odot}$  in the low and high metallicity components respectively and that  $Z_*$  is  $0.02 Z_{\odot}$ .

## 5. Discussion

Using a sample of H II galaxies of unprecedented size (about 400 objects) in which the oxygen abundances have been obtained using the temperature derived from the  $[\text{O III}] \lambda 4363/5007$  line ratio, we have confirmed the impressive trends and extremely strong correlations found in diagrams relating line ratios and  $\text{H}\beta$  equivalent width that we already found in previous studies (SL96 and SSL01). The He II  $\lambda 4686$  line is present at a level of 1 – 3 % of  $\text{H}\beta$  in a large number of H II galaxies, roughly half of the galaxies where the signal-to-noise was sufficient to detect and measure this line (which often appears on top of a Wolf-Rayet bump in the spectra). This line is present in

the entire range of  $\text{H}\beta$  equivalent widths, and its intensities show no correlations neither with  $EW(\text{H}\beta)$  nor with metallicity. The increase of  $[\text{N II}] \lambda 6584 / [\text{O II}] \lambda 3727$  with decreasing  $EW(\text{H}\beta)$ , already noted by SSL01, is clearly seen (although more dispersed than some other trends).

So far, analysis of emission line trends in H II galaxies made use of grids of photoionization models, but without attempting to propose a sequence of evolutionary models reproducing the observed trends.

Taking advantage of the large size of our sample and of the fact that the metallicities were determined in a direct and independent way, we divided our sample in three metallicity bins. We considered each bin separately, trying to find under what conditions a sequence of photoionization models, taking into account the time evolution of the ionizing cluster, reproduces all the observational diagrams adequately. In such an exercise, we used only very simple prescriptions, justified if possible by arguments related with what is known of the physics of these objects.

We have found that the simple model of an adiabatic expanding bubble gives rise to an increase of the  $[\text{O I}] \lambda 6300 / \text{H}\beta$  ratio with time, reaching the highest values observed in about 5 Myr. The presence of an older, non ionizing stellar population that contributes to the continuum at  $\text{H}\beta$  has been attested by direct studies of the stellar features in the continuum of H II galaxies. The characteristics of such an old population should of course be independent of the age of the most recent burst of star formation. Since the contribution of this old population to the stellar continuum at  $\text{H}\beta$  is proportionally larger for younger starbursts, such an underlying population is not sufficient to reproduce quantitatively the observed trends in the  $[\text{O III}] \lambda 5007 / \text{H}\beta$  vs.  $EW(\text{H}\beta)$ ,  $[\text{O III}] \lambda 5007 / [\text{O II}] \lambda 3727$  vs.  $EW(\text{H}\beta)$ , and He I  $\lambda 5876 / \text{H}\beta$  vs.  $EW(\text{H}\beta)$  diagrams. The observational data require that the covering factor  $f$  of the ionizing source by the emitting gas decreases with time. A reasonable fit to the observations is provided assuming an aperture correction of 0.5 to the models and an exponentially decreasing covering factor, with an e-folding time of 3 Myr, associated with an old population contributing at a level equal to the  $\text{H}\beta$  continuum produced by the young stars at zero age. That the covering factor of giant H II regions is smaller than unity and depends on the evolutionary stage of the region has already been suggested by Castellanos et al. (2002) from the study of a limited number of objects in spiral galaxies. What we find here is that there seems to be an universal law for the temporal variation of the covering factor. The physical reason underlying such a law could be linked to departure from spherical symmetry and blowout or to shell fragmentation (see Tenorio-Tagle et al. 1999).

We find that the He II  $\lambda 4686$  nebular line emission in H II galaxies occurs too frequently and in too wide a range of  $EW(\text{H}\beta)$  to be attributable to either the hard radiation field from Wolf-Rayet stars, as was suggested by Schaerer (1996, 1998), or the X-rays produced by current evolutionary synthesis models of young starbursts (Cerviño et al. 2002). Assuming that the He II  $\lambda 4686$  line is due to pho-

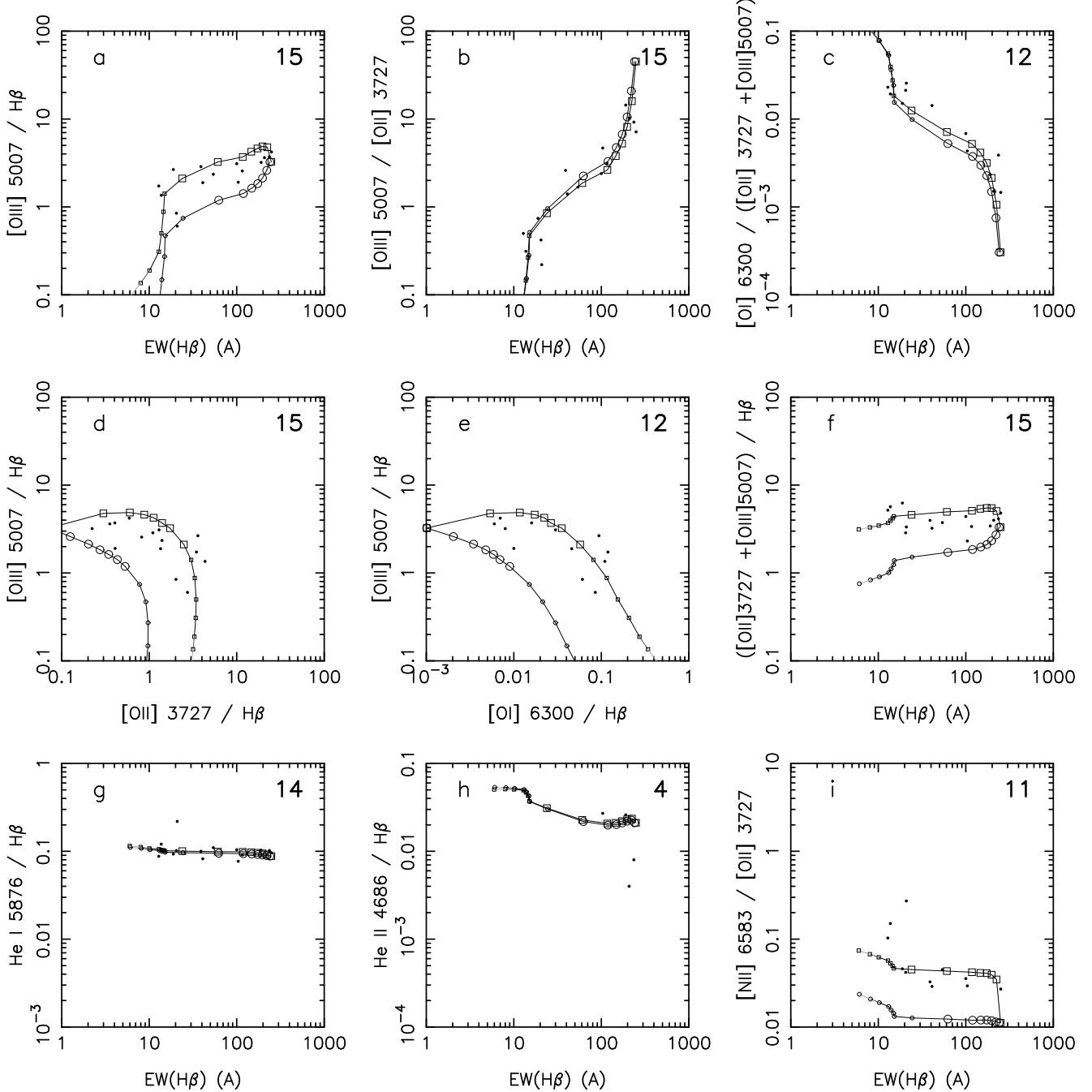


**Fig. 6.** The data points correspond to the “low” metallicity bin, The data points have  $O/H < 3 \times 10^{-5}$ . The model sequence represented by circles corresponds to sequence L4: metallicity  $Z = 0.02 Z_{\odot}$ , expanding bubble with varying covering factor and old underlying population included, and additional ionization by X-rays. The model sequence represented by squares corresponds to the composite sequence L5, i.e. same as L4 but including the effect of self-enrichment (for complete descriptions of the model sequences, see text and Table 1).

to ionization by a hot plasma at a temperature of  $10^6$  K, a total X-ray luminosity of  $10^{40} - 4 \times 10^{40} \text{ erg s}^{-1}$  is required for at least half of the sources. In some of the objects, the observed He II  $\lambda 4686$  nebular emission could actually be due to harder X-rays produced either by massive binaries or by supernova remnants from previous generations of stars in the age range of 10 – 50 Myr (Van Bever

& Vanbeveren 2000). Upcoming X-ray spectroscopy and imaging will help clarify the matter in the near future.

Our evolutionary sequences of models fail to reproduce perfectly the  $[O \text{ III}] \lambda 5007/H\beta$  vs.  $[O \text{ II}] \lambda 3727/H\beta$  and  $[O \text{ III}] \lambda 5007/H\beta$  vs.  $[O \text{ I}] \lambda 6300/H\beta$  diagrams for the intermediate and low metallicity bins, if the chemical composition is homogeneous and identical to the one of the gas which gave birth to the young stars. The col-

litionally excited lines are slightly – but significantly – too weak with respect to the observations. This problem had been noted before (SSL01), but here it is more visible due to the fact that we compare models with objects of similar metallicity. One way to understand the discrepancy is to postulate the existence of an additional heating mechanism. It is unlikely that this heating agent could be dust, or shocks produced by the energy released by winds and supernovae from the latest burst of star formation. Planetary nebulae and hot white dwarfs from earlier generations of stars would also be far from sufficient. The hypothesis of shock heating due either to stellar winds from previous generations of stars, or to cloud-cloud collisions needs to be investigated. However, another option to explain these emission line diagnostic diagrams is to invoke chemical inhomogeneities. Chemical inhomogeneities are expected in regions experiencing mass loss and supernova explosions from massive stars. The question is in what form is the newly synthesized matter, and how much of it has escaped the nebula. The problem is far from being settled at present (Roy & Kunth 1995; Tenorio-Tagle 1996; Silich & Tenorio-Tagle 1998; Mac Low & Ferrara 1999; Ferrara & Tolstoy 2000). So far direct evidence for self-enrichment has been scarce (see Kobulnicky (1999) for a review), but the fact that  $[\text{N II}] \lambda 6584 / [\text{O II}] \lambda 3727$  increases as  $EW(\text{H}\beta)$  decreases, especially in the intermediate and low metallicity bins of our sample, argue for the existence of self-enrichment in nitrogen on timescales of a few Myr. Of course, this in itself does not argue for any self-enrichment in oxygen, since the nitrogen and oxygen donors are different (see Matteucci & D’Ercole (1999) for a review). Given that the fate of the elements is still not well understood, we have felt it instructive to investigate the effect of inhomogeneous metallicity on the emission line diagnostic diagrams. We found that for the intermediate metallicity bin, a combination of two models with abundances  $Z_{\text{neb}} = 0.2 Z_{\odot}$  and  $0.05 Z_{\odot}$  leads to good agreement with the observations, but other solutions are likely possible as well. For the low metallicity bin our models indicate that a qualitatively similar composite model would be acceptable. The scatter of observational points in that bin is larger than in the other bins. This can be attributed to the small number of points in that bin and also to the fact that the effects of self-enrichment become more drastic at low metallicity. It is only for our high metallicity bin that there is a priori no need to invoke self-enrichment in oxygen, since the diagrams are satisfactorily reproduced for models with homogeneous chemical composition. However, chemical inhomogeneities, if present, are expected to have a smaller impact, due to the fact that  $[\text{O III}] \lambda 5007 / \text{H}\beta$  and  $[\text{O II}] \lambda 3727 / \text{H}\beta$  are not so dependent on metallicity for  $Z_{\text{neb}}$  between  $0.2 - 1 Z_{\odot}$  (see e.g. Stasińska 2002).

Finally, it is worth of noting that our prescriptions for the time dependence of the covering factor and of the degree of inhomogeneity were tailored to reproduce the emission line sequence of H II galaxies. On the other hand, the time dependence of the radius of the expand-

ing bubble is exactly the one predicted by the theory of supernova- and wind-blown bubbles. The size of the bubble required to reproduce the observational diagrams corresponds rather well with the prediction using the energy available from stellar winds and supernovae computed in population synthesis models. It is most encouraging that emission line diagnostics of H II galaxies confirm, on a statistical basis, the predictions of theories on stellar evolution, stellar populations and dynamical interaction with the interstellar medium. However, our interpretation should be compared to detailed modeling of selected objects in the entire sequence of  $EW(\text{H}\beta)$ . In particular, it would be important to compare the ages derived directly from the analysis of the stellar UV light with those implied by our interpretation of the emission line diagrams, and to use Wolf-Rayet stars as independent clocks. So far, only a handful of galaxies from our sample have been studied in such a way (Mas-Hesse & Kunth 1999), and the comparison is not conclusive.

*Acknowledgements.* It is a pleasure to thank Ryszard Szczerba, Laerte Sodr , Daniel Schaerer, Claus Leitherer, Miguel Cervi o, Polychronis Papaderos and the referee, Rosa Gonz lez-Delgado, for very fruitful discussions at various stages of this investigation. Y. I. acknowledges the support of the Observatoire de Paris, where part of this work was carried out and the Swiss SCOPE 7UKPJ62178 grant. The Sloan Digital Sky Survey (SDSS) is a joint project of The University of Chicago, Fermilab, the Institute for Advanced Study, the Japan Participation Group, the Johns Hopkins University, the Los Alamos National Laboratory, the Max-Planck-Institute for Astronomy (MPIA), the Max-Planck-Institute for Astrophysics (MPA), New Mexico State University, Princeton University, the United States Naval Observatory, and the University of Washington. Funding for the project has been provided by the Alfred P. Sloan Foundation, the Participating Institutions, the National Aeronautics and Space Administration, the National Science Foundation, the U.S. Department of Energy, the Japanese Monbukagakusho, and the Max Planck Society.

## References

- Allende Prieto, C., Lambert, D. L., & Asplund, M. 2001, *ApJ*, 556, L63
- Anders, E., & Grevesse, N. 1989, *Geochim. Cosmochim. Acta*, 53, 197
- Bernl hr, K. 1993, *A&A*, 268, 25
- Bresolin, F., Kennicutt, R. C., Jr., & Garnett, D. R. 1999, *ApJ*, 510, 104
- Calzetti, D., Kinney, A. L., & Storchi-Bergmann, T. 1994, *ApJ*, 429, 582
- Castellanos, M., Diaz, A. I., & Tenorio-Tagle, G. 2002, *ApJ*, 565, L79
- Cervi o, M. 2000, *Rev.Mex.Astron.Astrofis.*, 9, 283
- Cervi o, M., & Mas-Hesse, J. M. 1994, *A&A*, 284, 749
- Cervi o, M., Luridiana, V., & Castander, F. J. 2000, *A&A*, 360, 5
- Cervi o, M., Mas-Hesse, J. M., & Kunth, D. 2002, *A&A*, 392, 19
- Charlot, S., & Longhetti, M. 2001, *MNRAS*, 323, 887

- Cid Fernandes, R., Jr., Dottori, H. A., Gruenwald, R. B., & Viegas, S. M. 1992, *MNRAS*, 255, 165
- Dopita, M. A., & Evans, I. N. 1986, *ApJ*, 307, 431
- Dopita, M. A., Kewley, L. J., Heisler, C. A., & Sutherland, R. S. 2000, *ApJ*, 542, 224
- Ferrara, A., & Tolstoy, E. 2000, *MNRAS*, 313, 291
- García-Vargas, M. L., & Diaz, A. I. 1994, *ApJS*, 91, 553
- García-Vargas, M. L., Bressan, A., & Diaz, A. I. 1995, *A&AS*, 112, 13
- García-Vargas, M. L., González-Delgado, R. M., Perez, E., Alloin, D., Diaz, A., & Terlevich, E. 1997, *ApJ*, 478, 112
- Gordon, K. D., Calzetti, D., & Witt, A. N. 1997, *ApJ*, 487, 625
- Guseva, N. G., Izotov, Y. I., & Thuan, T. X. 2000, *ApJ*, 531, 776
- Guseva, N. G., Izotov, Y. I., Papaderos, P., et al. 2001, *A&A*, 378, 756
- Hillier, D. J., & Miller, D. L. 1998, *ApJ*, 496, 407
- Izotov, Y. I., & Thuan, T. X. 1998, *ApJ*, 500, 188
- Izotov, Y. I., Thuan, T. X., & Lipovetsky, V. A. 1994, *ApJ*, 435, 647
- Izotov, Y. I., Thuan, T. X., & Lipovetsky, V. A. 1997, *ApJS*, 108, 1
- Izotov, Y. I., Chaffee, F. H., Foltz, C. B., et al. 1999, *ApJ*, 527, 757
- Izotov, Y. I., Chaffee, F. H., & Green, R. F. 2001a, *ApJ*, 562, 727
- Izotov, Y. I., Chaffee, F. H., & Schaerer, D. 2001b, *A&A*, 378, L45
- Kobulnicky, H. A. 1999, in *Wolf-Rayet Phenomena in Massive Stars and Starburst Galaxies*, Proceedings IAU Symposium No. 193, eds. K. A. van der Hucht, G. Koenigsberger & P. R. J. Eenens, p. 670
- Kong, X., & Cheng, F. Z. 1999, *A&A*, 351, 477
- Kunth, D., & Östlin, G. 2000, *A&A Rev.*, 10, 1
- Kurucz, R. L. 1991, in *Stellar Atmospheres: Beyond Classical Limits*, ed. L. Crivellari, I. Hubeny, & D. G. Hummer (Dordrecht: Kluwer), 441
- Leitherer, C., Schaerer, D., Goldader, J. D., et al. 1999, *ApJS*, 123, 3
- Lipovetsky, V. A., Chaffee, F. H., Izotov, Y. I., et al. 1999, *ApJ*, 519, 177
- Loose, H.-H., & Thuan, T.X. 1985, in "Star-Forming Dwarf Galaxies and Related Objects", Kunth, D., Thuan, T.X., Van, T.T. (eds.). Paris: Editions Frontières, p.73
- Mac Low, M.-M., & Ferrara, A. 1999, *ApJ*, 513, 142
- Maíz-Apellániz, J., Muñoz-Tuñón, C., Tenorio-Tagle, G., & Mas-Hesse, J. M. 1999, *A&A*, 343, 64
- Masegosa, J., Moles, M., & Campos-Aguilar, A. 1994, *ApJ*, 420, 576
- Mas-Hesse, J. M., & Kunth, D. 1991, *A&AS*, 88, 399
- Mas-Hesse, J. M., & Kunth, D. 1999, *A&A*, 349, 765
- Matteucci, F., & D'Ercole, A. 1999, in *Wolf-Rayet Phenomena in Massive Stars and Starburst Galaxies*, Proceedings IAU Symposium No. 193, eds. K. A. van der Hucht, G. Koenigsberger & P. R. J. Eenens, p. 679
- McCall, M. L., Rybski, P. M., & Shields, G. A. 1985, *ApJS*, 57, 1
- McGaugh, S. S. 1991, *ApJ*, 380, 140
- Meynet, G., Maeder, A., Schaller, G., Schaerer, D., & Charbonnel, C. 1994, *A&AS*, 103, 97
- Moy, E., Rocca-Volmerange, B., & Fioc, M. 2001, *A&A*, 365, 347
- Olofsson, K. 1989, *A&AS*, 80, 317
- Papaderos, P., Loose, H.-H.; Thuan, T. X., & Fricke, K. J. 1996, *A&AS*, 120, 207
- Papaderos, P., Izotov, Y. I., Fricke, K. J., Thuan, T. X., & Guseva, N. G. 1998, *A&A*, 338, 43
- Papaderos, P., Fricke, K. J., Thuan, T. X., Izotov, Y. I., & Nicklas, H. 1999, *A&A*, 352, 57
- Pauldrach, A. W. A., Hoffmann, T. L., & Lennon, M. 2001, *A&A*, 375, 161
- Pilyugin, L. S. 2000, *A&A*, 362, 325
- Popescu, C. C., & Hopp, U. 2000, *A&AS*, 142, 247
- Raimann, D., Bica, E., Storchi-Bergmann, T., Melnick, J., & Schmitt, H. 2000, *MNRAS*, 314, 295
- Roy, J.-R., & Kunth, D. 1995, *A&A*, 294, 432
- Sargent, W. L., & Searle, L. 1970, *ApJ*, 162, 155
- Schaerer, D. 1996, *ApJ*, 467, L17
- Schaerer, D. 1998, *Highlights of Astronomy*, 11a, 134
- Schaerer, D., & de Koter, A. 1997, *A&A*, 322, 598
- Schaerer, D., & Vacca, W. D. 1998, *ApJ*, 497, 618
- Schmutz, W., Leitherer, C., & Gruenwald, R. 1992, *PASP*, 104, 1164
- Silich, S. A., & Tenorio-Tagle, G. 1998, *MNRAS*, 299, 249
- Stasińska, G. 1999, in "Dwarf galaxies and Cosmology", Eds. T.X. Thuan, C. Balkowski, V. Cayatte, J. Tran Thanh Van, (editions frontieres), p. 259
- Stasińska, G. 2002, *Rev.Mex.Astron.Astrofis.*, 12, 62
- Stasińska, G., & Leitherer, C. 1996, *ApJS*, 107, 661 (SL96)
- Stasińska, G., & Schaerer, D. 1999, *A&A*, 351, 72
- Stasińska, G., & Szczerba, R. 2001, *A&A*, 379, 1024
- Stasińska, G., Schaerer, D., & Leitherer, C. 2001, *A&A*, 370, 1 (SSL01)
- Stoughton, C., Lupton, R. H., Bernardi, M., et al. 2002, *AJ*, 123, 485
- Tenorio-Tagle, T. 1996, *AJ*, 111, 1641
- Tenorio-Tagle, G., Silich, S. A., Kunth, D., Terlevich, E., & Terlevich, R. 1999, *MNRAS*, 309, 332
- Terlevich, R., & Melnick, J. 1985, *MNRAS*, 213, 841
- Terlevich, R., Melnick, J., Masegosa, J., Moles, M., & Copetti, M. V. F. 1991, *A&AS*, 91, 285
- Thuan, T. X., Izotov, Y. I., & Foltz, C. B. 1999, *ApJ*, 525, 105
- Thuan, T. X., Izotov, Y. I., & Lipovetsky, V. A. 1995, *ApJ*, 445, 108
- Thuan, T. X., Izotov, Y. I., & Lipovetsky, V. A. 1997, *ApJ*, 477, 661
- Van Bever, J., & Vanbeveren, D. 2000, *A&A*, 358, 462
- van Zee, L., Salzer, J. R., & Haynes, M. P. 1998a, *ApJ*, 497, L1
- van Zee, L., Skillman, E. D., & Salzer, J. R. 1998b, *AJ*, 116, 1186
- Veilleux, S., & Osterbrock, D. E. 1987, *ApJS*, 63, 295
- Weaver, R., Castor, J., McCray, R., Shapiro, P., & Moore, R. 1977, *ApJ*, 218, 377
- Zackrisson, E., Bergvall, N., Olofsson, K., & Siebert, A. 2001, *A&A*, 375, 814